Facile synthesis and exfoliation of micro-sized LDH to fabricate 2D membranes towards Mg/Li separation

Biao Li, Juanjuan Peng, Menghan Li, Zeya Yang, Jun Lu and Jingbin Han*

State Key Laboratory of Chemical Resource Engineering, Beijing Advanced Innovation Center for Soft Matter Science and Engineering, Beijing University of Chemical Technology, Beijing 100029, P. R. China

Author Information

∗ Corresponding authors.

Phone: +86-10-64412131.

Fax: +86-10-64425385.

E-mail: hanjb@mail.buct.edu.cn.

Abstract:

Two-dimensional (2D) membranes have demonstrated potential for molecular separation; however, their applicability for Li/Mg ion separation has been restricted by their negatively-charged and easily-swellable properties in water. Moreover, their practical application has been hindered by the challenge of producing significant quantities of single-layer nanosheets. To overcome these challenges, we have developed a scalable method for synthesizing micro-sized nitrate ZnAl layered double hydroxide (LDH) and subsequent exfoliating to yield monolayer nanosheets for the construction of 2D membranes. The sub-nanometer channels of the LDH membrane is positively charged, which prevents the passage of magnesium ions. These channels also impede the flow of magnesium ions that are more difficult to dehydrate. As a result, the LDH membranes exhibit robust lithium-magnesium separation ability, with a separation ratio of 6 (Li/Mg). This work provides a method for producing high-quality LDH nanosheets and validates the enormous potential of LDH membranes in the field of lithium-magnesium separation.

KEYWORDS: ZnAl-LDH; monolayer nanosheets; 2D membrane; ion sieving

1. Introduction

Lithium is a critical element in Li-ion batteries (LiBs), ceramics, lubricants, and the nuclear industry.[1] Especially in the field of LiBs, it is predicted that the continuous development of portable electronic devices and new energy vehicles will significantly increase the demand for lithium, making it a geopolitically significant resource.[2] Brines is an important source of lithium, accounting for 58% of the world's proven reserves.[3] Unfortunately, current lithium extraction technologies, including precipitation, salting, and solvent extraction, are plagued by time-consuming and costly processes,[4-7] because there are a large number of other ions in brines with similar chemical properties and structures to lithium, including Mg^{2+} (normally the highest), K^{+}, and Na^{+}. The development of new, energy-efficient separation techniques, especially for Li/Mg separation, is urgently required.[8]

Membrane technology is an attractive alternative for aqueous lithium separation due to its high efficiency, simple process, and low energy consumption.[9-11] Two-dimensional (2D) membranes, in particular, have demonstrated excellent potential in the field of ion separation, introducing new possibilities for achieving higher performance separation.[12-16] Size screening is one of the important mechanisms of separation. The robust sub-nanometer channel is the basis for the membrane to achieve a stable separation performance.[4,17-19] Additionally, the charged properties of membranes play a crucial role in separating substances with different charges.[2,20-22] For lithium-magnesium separation, a membrane with positively charged sub-nanometer channels will more strongly repel the passage of magnesium ions, thus showing the enhanced separation effect of lithium and magnesium.[8,23-26] However, mostly two-dimensional materials, such as GO,[18] MXene,[16] vermiculite,[19] etc., are negatively charged

and have swelling problems in water,[27,28] which will reduce the ability of Li/Mg separation. In addition, exfoliating bulk 2D materials into nanosheets is necessary for building layered membranes, but it involves harsh conditions, making it a complicated process that limits the development of these membranes.

Layered double hydroxides (LDHs) is a typical anionic intercalated 2D material that has a positively charged laminate and shows high stability in water, indicating that it is a potential material platform for constructing a Li/Mg separation membrane.[29,30] Although the exfoliation process of LDHs is relatively moderate, large-scale preparation of high-quality nanosheets remains a challenge.[31,32] The "top-down" method is a common way to obtain LDH nanosheets.[29,33] In general, urea is used as the alkali source to obtain CO_3-LDH by hydrothermal reaction, and then NO_3-LDH is obtained by acid-salt exchange to facilitate delaminating. However, this process is atomically uneconomical because it consumes a lot of nitrate (the mass ratio of nitrate to LDH is 127) and is time-consuming (at least 96 h) and low-yielding. Although there are bottom-up methods for directly synthesizing LDH nanosheets,[34,35] the size is generally below tens of nanometers, which is not suitable for constructing membranes. A method to obtain high-quality LDH nanosheets in large quantities at a low cost will aid in their wide-scale application. The consensus is that the direct synthesis of micron-sized NO_3-LDH will greatly reduce the consumption of reagents and time. However, this is difficult because CO_3^{2-} has a stronger affinity with LDH laminates.[36,37] Generally, even if the introduction of carbonate-containing reagents is avoided during the synthesis process, CO_3^{2-} can still be detected in the final product because of the strong affinity between LDH host layer and CO_3^{2-} ions. Previous research has revealed that the

different metal elements in LDH laminate may affect its adsorption of carbon dioxide. This suggests that altering the kind of laminated metal may reduce the pollution of carbonate and facilitate the formation of pure nitrate LDH.

The present study aimed to synthesize pure nitrate LDHs, including CoAl, ZnAl, MgAl, and NiAl LDH, through a one-step method with large particle size. Among the synthesized compounds, ZnAl-LDH was found to be less prone to carbonate contamination, optimizing the synthesis process for micron-sized nitrate LDH. The ZnAl-LDH platelets obtained from this method were cost-effective and easily exfoliated into single-layer nanosheets, suitable for constructing layered membranes with stable sub-nanometer channels that bear a positive charge. The positively charged character of LDH membrane makes it more repellent to magnesium ions. In addition, the LDH membrane does not swell in water and has stable sub-nanometer channels. It is difficult for magnesium ions, which are hardness to dehydrate, to pass through the stable sub-nanometer channels, giving the LDH membranes good and sustained lithium-magnesium separation capabilities.

2. Experimental section

2.1 Reagents and Materials.

All chemicals were used without further purification. $Zn(NO_3)_2 \cdot 6H_2O$, $Mg(NO_3)_2 \cdot 6H_2O$, $Co(NO_3)_2 \cdot 6H_2O$, $Ni(NO_3)_2 \cdot 6H_2O$, $Al(NO_3)_3 \cdot 9H_2O$, $MgCl_2 \cdot 6H_2O$, $FeCl_3 \cdot 6H_2O$, NaCl, LiCl, ethanol commercially available from TJ-jinteng company. Formamide, acetone and n-hexane were purchased from Macklin company. Deionized water was used in all the experiments.

2.2 Methods

Preparation of (*M*)Al-LDH

The (*M*)Al–LDH (*M* = Mg, Zn, Co and Ni) nanoplatelets were synthesized according to the separate nucleation and aging steps method reported by our group.[38] Typically, $Al(NO_3)_3 \cdot 9H_2O$ (100 mmol), $M(NO_3)_2$ (50 mmol) were dissolved in 500 mL deionized water denoted as solution A. NaOH (150 mol) were dissolved 1000 mL deionized water denoted as solution B. Solution A and B were mixed together simultaneously in a colloid mill for 1 minute at a rotating rate of 3000 rpm. Then the collected colloid was transferred into a stainless Teflon-lined autoclave and kept in oven at 110 °C for 24 h for crystallization. The product was washed three times with water and once with ethanol, respectively. Finally, the moist product is sealed and preserved.

Preparation of LDH nanosheets

X gram (*X* = 0.25~5) ZnAl-LDH was mixed with 100 ml formamide, followed by aging using a mechanical shaker for 5 min. Then the mixture was sonicated for 1 hour to achieve the preparation of LDH nanosheets.

Preparation of LDH laminar membrane

Vacuum-assisted filtration methods was used to prepare LDH laminar membrane. Typically, the LDH colloidal solution (0.2 g/100 ml) was diluted 100 times with water and filtrated under 1 bar vacuum on a nylon membrane with an effective diameter of 40 mm. Then the as-fabricated LDH membrane was dried in a vacuum oven at 60 °C for 24 h.

Ion permeation test

The ion permeation tests were conducted using a two-compartment electrochemical cell fabricated in-house. The membrane was sandwiched between two electrochemical cells. Then, the same concentration of salt solution to be measured was injected into the two cells. And the

I-V properties were measured with a pair of Ag/AgCl electrodes and recorded by CHI 660D electrochemical workstation at the mode of linear sweep voltammetry. Membrane conductance can be calculated according to the slope of the I-V curve.

The ion diffusion experiment driven by a concentration gradient was also carried out in an H-type cell. The difference is that 0.1 M salt solution and deionized water are injected into the two cells. The conductivity meter was used to monitor the change of salt concentration on the deionized water side.

Theoretical calculations

The DFT calculations in this work were performed using the CASTEP module in the Materials Studio version 8 software package. The single ion, water molecule and hydrated ion models were built and optimized. After the energy optimization of hydrated ions is completed, the differential charge density diagram can also be obtained. Besides, the final energy of the corresponding system ($E_{M^{n+}}$, $E_{((H_2O)_n)}$, $E_{(M^{n+}(H_2O)_n)}$) was calculated. And the binding energy of water and ions can be calculated by the formula (2).[38]

$$M^{n+}(H_2O)_2 \rightleftharpoons M^{n^+} + (H_2O)_n \quad (1)$$

$$E_{Bining} = E_{M^{n+}} + E_{((H_2O)_n)} - E_{(M^{n+}(H_2O)_n)} \quad (2)$$

The electrostatic double-layer (EDL) interaction (U_{EDL}) between ions and membrane was calculated using the SEI technique.[18,22] The SEI method integrates the interaction energy per unit area (E_{EDL}) between the planar membrane surface and the hydrated ion to consider the overall interaction energy (U_{EDL}), which can be calculated by formula (3). The interaction energy per unit area (E_{EDL}) between ions and membrane can be expressed as (4).

$$U(D) = \iint E(h)\,dA \quad (3)$$

$$E_{EDL}(h) = \frac{\epsilon_0 \epsilon_r \kappa}{2}\left(\psi_s^2+\psi_p^2\right)\left(1-\coth(\kappa h)+\frac{2\psi_s\psi_p}{\left(\psi_s^2+\psi_p^2\right)}\operatorname{cosech}(\kappa h)\right) \quad (4)$$

Where, ϵ_0 is permittivity in vacuum, ϵ_r is relative dielectric permeability of the solvent, ψ_s was surface potential of hydrated ions, ψ_P is surface potential of LDH membrane,κ is the inverse Debye screening length, and *h* is the distance between LDH membrane and ions, respectively.

Characterization techniques

XRD patterns were recorded by a UItima III XRD diffractometer at 40 kV, 30 mA with Cu Kα radiation (λ = 0.1542 nm). The morphology of LDHs and LDH membranes were observed by SEM (Zeiss SUPRA 55) and TEM (JEM-2100). AFM images were captured on a Bruker Dimension Icon atomic force microscope. The zeta-potential and particle size distribution of the solutions was measured by a laser particle size analyzer (Zetasizer Nano ZS 90, USA). FT-IR spectra were recorded on a Nicolet 6700 spectrometer (Thermo Fisher Nicolet, USA) at room temperature. Thermogravimetric and mass spectrometric (TG-MS) analysis were performed simultaneously using the STA7300 with Skimmer coupled to a quadruple mass spectrometer GAM200. The salt concentration was measured according to the conductivity of salt solution by a DDS-307A (INESA) conductivity meter.

3. Results and discussion

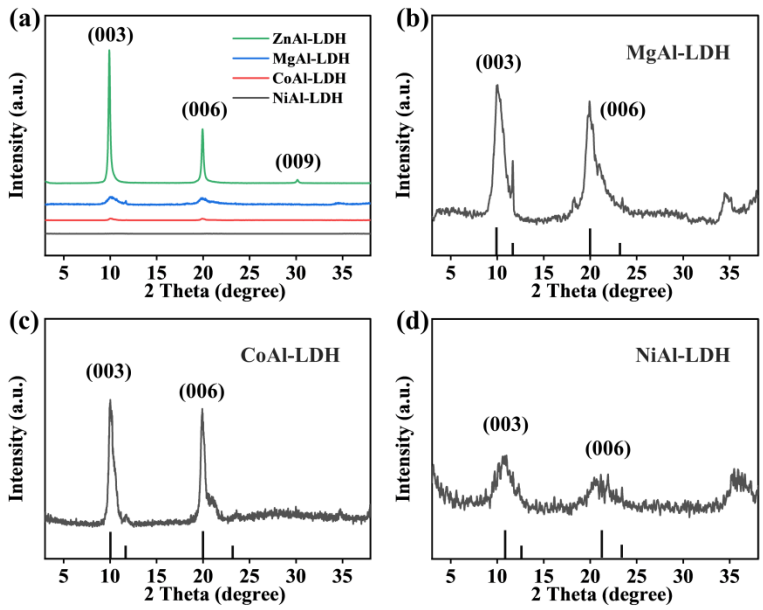

Figure 1. XRD patterns of (a) (*M*)Al-LDH (*M* = Zn; Mg; Co and Ni); and expanded XRD patterns of (b) MgAl-LDH; (c) CoAl-LDH; (d) NiAl-LDH.

Four kinds of LDHs (CoAl-LDH; MgAl-LDH; ZnAl-LDH; NiAl-LDH) were synthesized by the separate nucleation and aging steps method. Avoid using any carbonate-containing reagents to avoid carbonate ion contamination. In order to verify the interlayer anion species of the synthesized LDHs, XRD and IR analyses were carried out. Figure 1 shows the XRD pattern of four kinds of LDHs. For ZnAl-LDH, three single Bragg diffraction peaks at 10°, 20°, and 30° can be assigned to (003), (006), and (009) diffractions, which is consistent with the typical nitrate intercalated LDH. In the IR spectrum (Figure S1), the sharp peak at 1384 cm^{-1} can be attributed to the vibration of interlayer nitrate ions. However, for the other three LDHs, the appearance of twin peaks at about 10°, 11.5° and 20°, 23° in the XRD pattern (Figure 1b, c and d), which is attributed to (003) and (006) diffractions, respectively, indicates the presence of carbonate and nitrate intercalated LDH. Similarly, a strong peak attributed to CO_3^{2-} vibration at about 1360 cm^{-1} in the IR spectrum (Figure S1)

was also observed, indicating that CO_3^{2-} were present in these three LDHs. These results indicate that is easy to prepare pure nitrate intercalated ZnAl-LDH directly, while it is relatively difficult for CoAl-LDH, MgAl-LDH and NiAl-LDH. These later three LDH are more easily contaminated by carbonate ions.

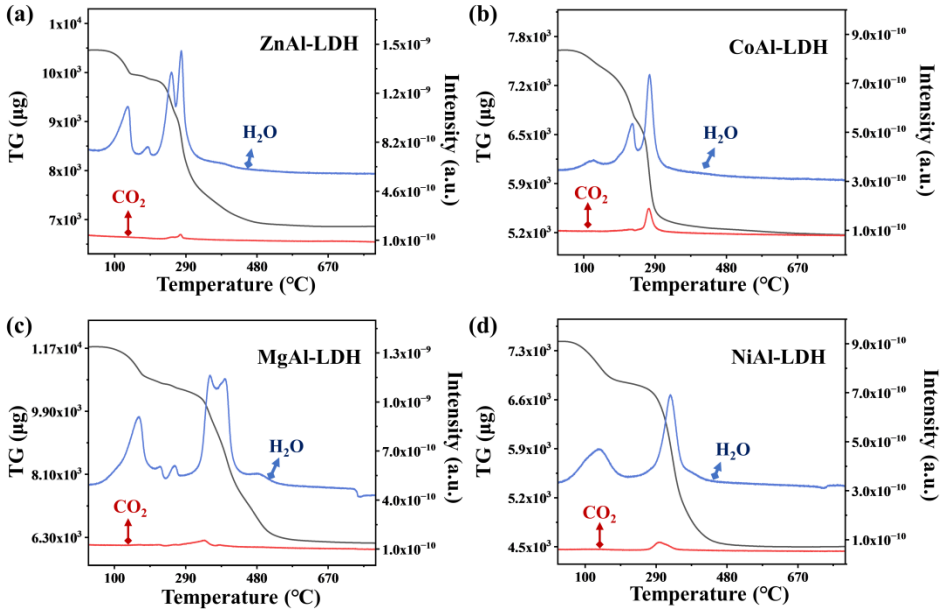

Figure 2. TG/MS spectrogram of (a) ZnAl-LDH; (b) CoAl-LDH; (c) MgAl-LDH; (d) NiAl-LDH.

The simultaneous TG-MS study (Figure 2) was performed on four kinds of LDHs to verify their adsorption of CO_2. As summarized in Figure S2a, the desorption temperatures of these four LDHs for CO_2 are: 255.5 °C for CoAl-LDH; 259.5 °C for ZnAl-LDH; 284.4 °C for NiAl-LDH; and 327.9 °C for MgAl-LDH. The desorption temperature is related to the binding strength of LDH to carbon dioxide species in the interlayer. The higher the desorption temperature is, the stronger the binding force between carbon dioxide species and LDH is.[39] This result shows that the adsorption of carbon dioxide species in ZnAl-LDH and CoAl-LDH is relatively weak. Further, the adsorption capacity of the four LDHs to carbon dioxide species

can be qualitatively analyzed by comparison with the value of carbon dioxide removal signal peak areas to be split by the starting mass. The adsorption capacity of ZnAl-LDH per unit mass for carbon dioxide species is the smallest compared with the other three LDHs (Figure S2b), which can also explain why ZnAl-LDH is less susceptible to carbonate pollution in the air.

In addition, in the process of homogeneous nucleation of ZnAl-LDH, the relative strong binding force between zinc and nitrate allows nitrate to participate in the nucleation process. At the onset of the process, two precursors $Zn_2(OH)_3NO_3$ and $Al(OH)_3$ are formed as illustrated in the following reaction equations, which can possibly explain why the synthesis of pure nitrate ZnAl-LDH is easier. Despite the lack of direct evidence, this understanding is consistent with previous work.[41] While for the other three LDHs, anion typically enters the main laminate interlayer by diffusion after the layered structure formed. Due to the strongest binding force between carbonate and the laminate, the inevitable carbonate pollution will lead to the formation of carbonate LDHs.

$$2Zn(NO_3)_2 + 3NaOH \rightarrow Zn_2(OH)_3NO_3 + 3NaNO_3;$$

$$Al(NO_3)_3 + 3NaOH \rightarrow Al(OH)_3 + 3NaNO_3;$$

$$Zn_2(OH)_3NO_3 + Al(OH)_3 \rightarrow Zn_2Al(OH)_6NO_3 \text{ (ZnAl-LDH)}$$

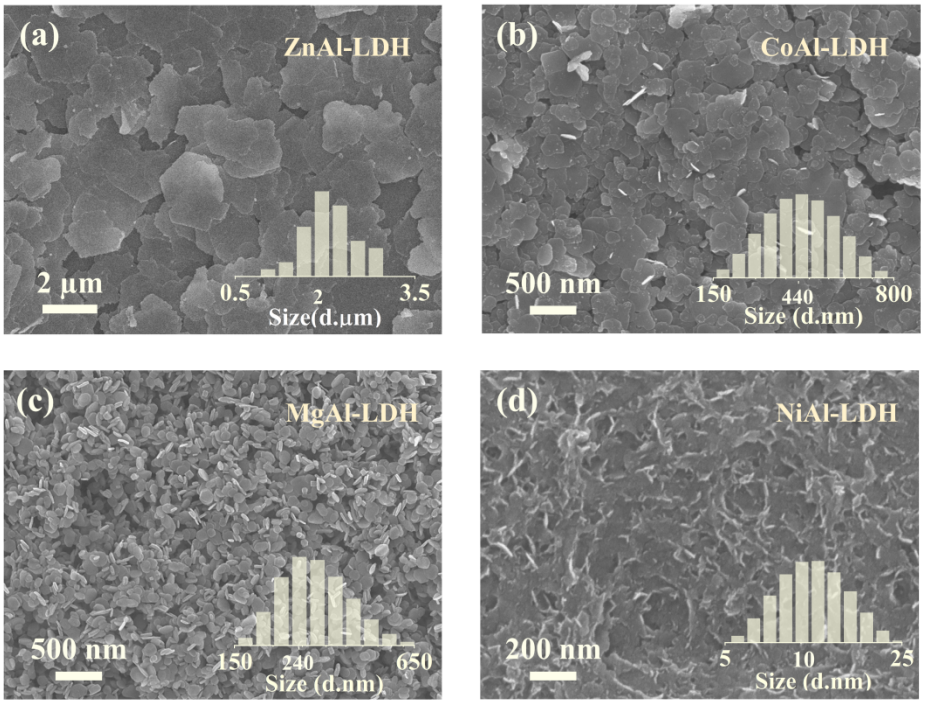

Figure 3. SEM images and particle size distribution of (a) ZnAl-LDH; (b) MgAl-LDH; (c) CoAl-LDH; (d) NiAl-LDH.

Figure 3 shows the SEM images and particle size analysis of four LDHs. ZnAl-LDH has an irregular sheet with a size distribution of about 2 μm, whereas CoAl-LDH, MgAl-LDH, and NiAl-LDH have size distributions of 440 nm, 240 nm, and 10 nm, respectively. This finding is surprising because the separate nucleation and aging steps method typically produces LDHs with nanometer-sized particles,[40] whereas urea-assisted hydrothermal synthesis produces LDHs with micron-sized particles.[33] This result shows that the change of metal elements in the laminate will produce LDHs of different sizes. The growth process of ZnAl-LDH was verified by SEM images (Figure S3) of different crystallization times. When the crystallization time is 0 h, the product is composed of small LDH grains and flakes. When the crystallization time is extended to 12 hours, micron-sized nanosheets are formed, and

small LDH grains are still attached to the edges of the nanoplates, suggesting that they are still growing. The larger nanoplates after 24 hours of crystallization verify that they were still growing at 12 hours of crystallization. Yet, the size of the LDHs does not grow as the crystallization period lengthens. These indicate that the growth of ZnAl-LDH is caused by the interlinking process of small grains (Figure S4), which also is verified by TEM images (Figure S5). With the increase in crystallization time, the thickness of ZnAl-LDH will not increase significantly. AFM and SEM (Figure S6) shows that the thickness of ZnAl-LDH nanoplate was about 25 nm, when the crystallization time is 24 hours.

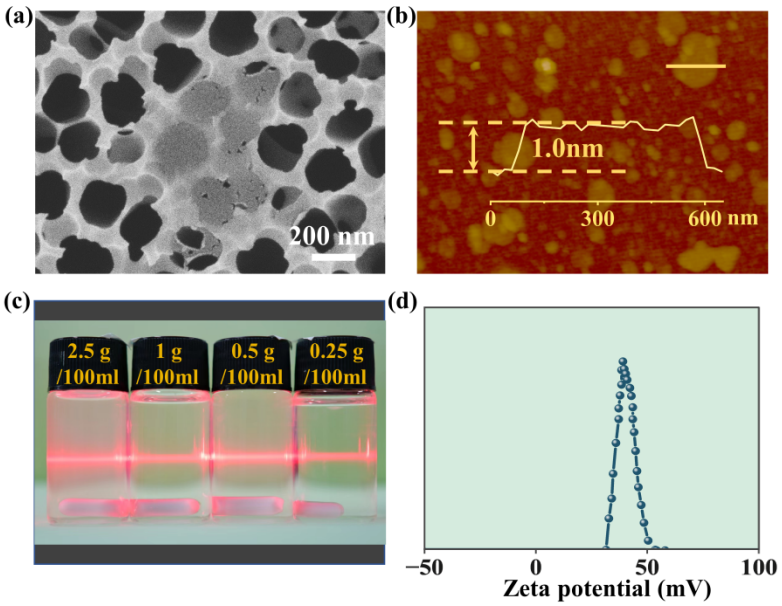

Figure 4. (a) SEM images of ZnAl-LDH nanosheets deposited on the anodic aluminum oxide (AAO) substrate; (b) AFM image of a monolayer LDH nanosheet; (c) Photographic image of colloidal suspension of exfoliated ZnAl-LDH nanosheets with different concentration; (d) The zeta potentials of ZnAl-LDH nanosheets solutions.

Formamide was used as a solvent to delaminate LDHs. Because carbonate-intercalated LDH are present in CoAl, MgAl and NiAl LDHs, exfoliation of these LDHs partially happens.

AFM (Figure S7) reveals nanosheets that are several nanometers or more than 10 nanometers thick. Obvious flocculent precipitation was observed after standing these three LDHs colloidal solution, which also indicates that there were unpeeled nanoplates in the obtained colloidal solution (Figure S8). Nevertheless, the exfoliation of ZnAl-LDH requires only 30 minutes of ultrasound due to its small thickness and large interlayer spacing. Figure 4 shows the SEM and AFM images of the exfoliated ZnAl-LDH nanosheets, which indicates that ZnAl-LDH exhibit an average thickness of 1 nm with lateral sizes in the range of 600 nm. LDH with concentration ranges from 0.25 g/100 ml to 5 g/100 ml can be exfoliated, and LDHs with high concentrations can form gels after exfoliation (Figure S9) that can be used to prepare large quantities of nanosheets. Figure 4c shows that stripped LDH colloidal solutions has an obvious Tyndall effect with zeta potential of ~30 mV (Figure 4d). The preparation of ZnAl-LDH nanosheets by this strategy has the advantages of short time, low cost and large size of nanosheets (Figure S10).

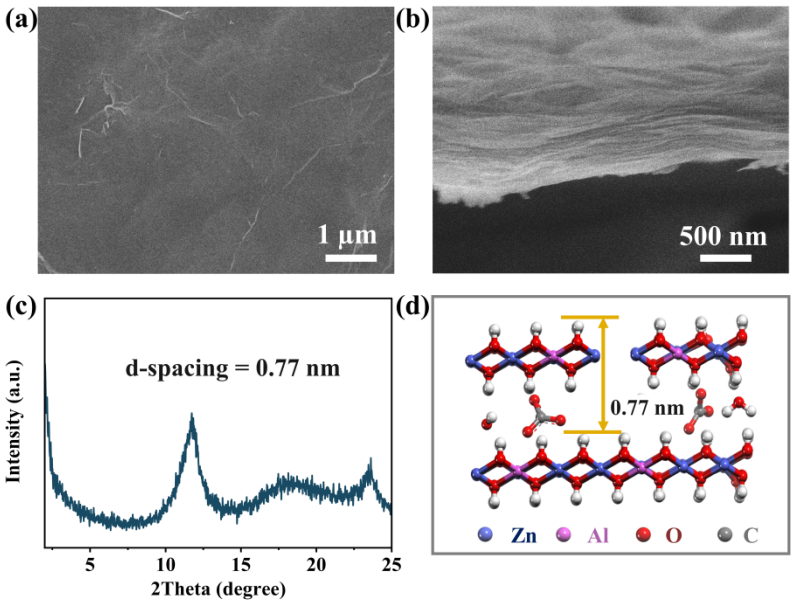

Figure 5. (a) and (b) Top-view and cross-section SEM images of LDH membrane; (c) XRD patterns of LDH membrane; (d) Structure diagram of cross-section LDH membrane.

Large monolayer nanosheets are considered the cornerstone for constructing layered membranes. The LDH membrane was prepared by vacuum-assisted filtration methods using the ZnAl-LDH nanosheets. As shown in Figure 5, the pores of the substrate (Figure S11) were completely covered after the deposition of LDH nanosheets, and the surface was defect-free. The obtained LDH self-supporting membrane is translucent and has certain flexibility (Figure S12). Figure S13 shows that elements such as Zn, Al, and O are evenly distributed. The cross-section SEM images exhibits a typical layered structure. And XRD pattern indicates that the interlayer spacing is 0.77 nm, which corresponds to the interlayer spacing of carbonate LDHs. This suggests that when the LDH membranes were assembled by LDH nanosheets, the carbonate from CO_2 dissolved in water with the strongest binding force was more likely to enter its interlayer.

Ion permeation test

To investigate the transmembrane properties of ions, the LDH membrane was clamped in a home-made electrochemical cell. Then, the current-voltage (I-V) curves across the membrane were measured by using a pair of Ag/AgCl electrodes. Figure 6 shows the I-V curves of the membrane in a series of KCl electrolytes with various concentrations and the corresponding transmembrane ionic conductance. In the high-concentration region (over 10^{-3} M), transmembrane ionic conductance is determined by the concentration and shows a linear relationship. When the KCl concentration is lower than 10^{-3}, the conductance gradually turns into a plateau due to the overlap of electrical double layer inside the nanochannels. Generally, typical surface-charge-governed ion transportation properties were revealed.

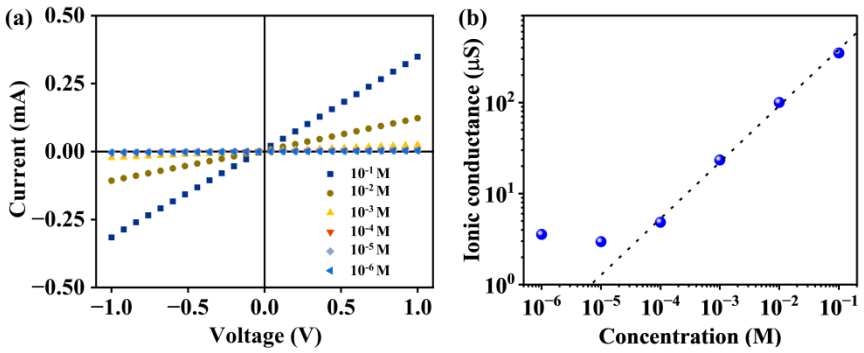

Figure 6. (a) Current-voltage curve of LDH membrane for KCl with different concentration; (b) Conductance versus salt concentration for LDH membrane.

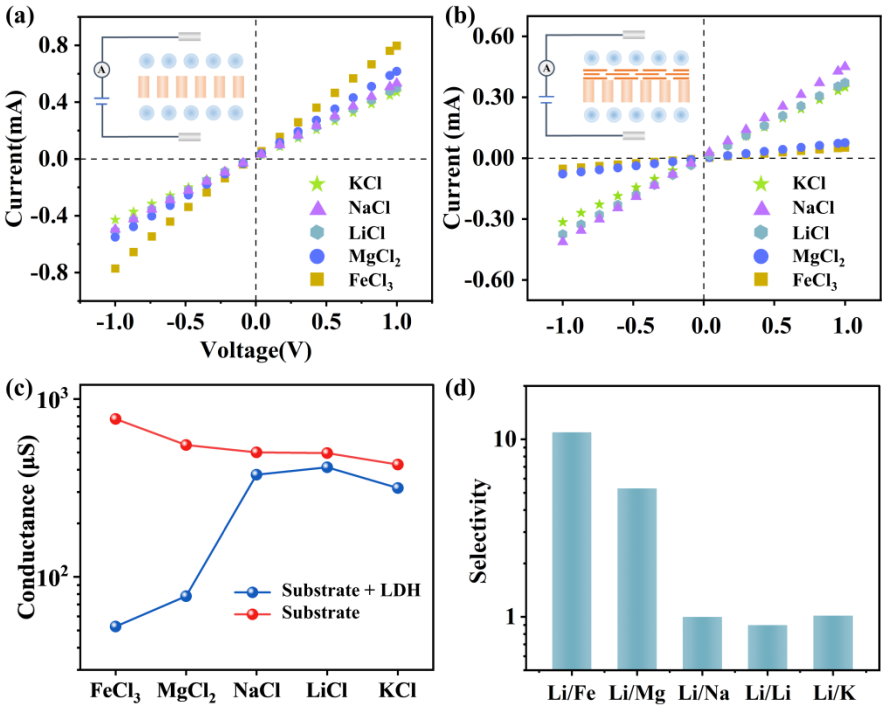

Figure 7. Current-voltage curve of (a) substrate and (b) substrate + LDH membrane for five salt solutions; (c) Conductance versus five salt for substrate and substrate+LDH membrane; (d) ion selectivity of LDH membrane.

Transmembrane properties of different salt (KCl, NaCl, LiCl, $MgCl_2$, $FeCl_3$) solutions were also assessed by measuring I-V curves. Ions pass through the membrane to generate current. Therefore, the higher the slope of the I-V curves, the faster the ion transmembrane rate would be. I-V curves of LDH membrane and substrate were recorded. As illustrated in

Figure 7a, b, all test ions exhibit a linearity in their I-V curves. And the I-V curve of LDH membrane for the five salts has a lower slope than the I-V curve of the substrate, which suggests that the LDH membrane delays the ion permeation. Furthermore, the hysteresis effect on different salt permeation is different, indicating that the membrane has ion permeation selectivity. Since the five electrolyte solutions have the same anion (Cl^-), the difference in I-V curves slope is mainly caused by cations. For Mg^{2+} and Fe^{3+}, the ionic conductance drops more than for K^+, Na^+, and Li^+ (Figure 7c). Especially for Fe^{3+}, Mg^{2+} ions decreased by 14.6 times and 7.1 times, respectively, while Li^+ only decreased by 1.2 times. It is suggested that the LDH membrane will hinder the permeation of Mg^{2+} and Fe^{3+} and allow the permeation of Li^+.

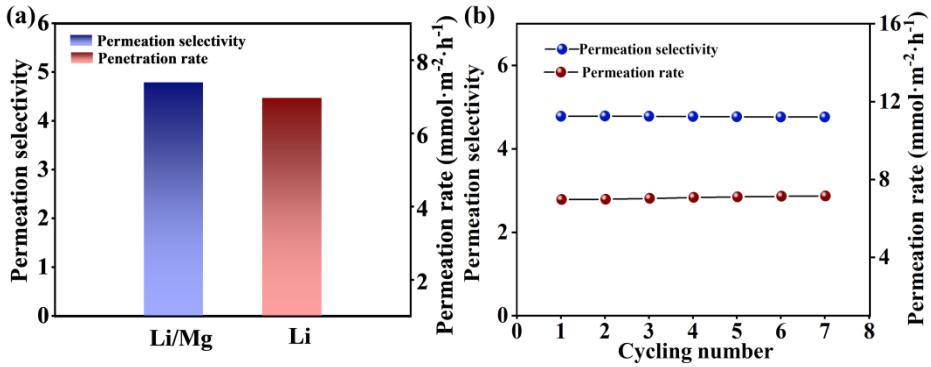

Figure 8. Ionic permeation of the LDH membranes in single salt solution systems. (a) Li^+ permeation rates vs. permeation selectivity (Li/Mg) of LDH membranes; (b) Long-term stability of the LDH membrane.

The ion diffusion experiment under a concentration gradient was also conducted. As shown in Figure 8a, the Li^+ and Mg^{2+} permeation rates through the LDH membrane are 7.0 mmol m^{-2} h^{-1} and 1.45 mmol m^{-2} h^{-1}, respectively, which is consistent with the conductivity test. Additionally, the LDH membrane displays long-term stability (Figure 8b) with an

average Li^+/Mg^{2+} selectivity of about 4.78 and a constant Li^+ permeation rate of 7 mmol m^{-2} h^{-1} for up to 7 cycle tests. This is attributed to the fact that the membrane is stable in water and will not swell and re-disperse, unlike the circumstance in GO membranes.[28] The interlayer spacing of LDH membranes in the dry state and after soaking in water for 5 days is consistent (Figure S14), indicating the stability of LDH nanochannels. Although the lithium-magnesium separation performance of this work did not reach the best level, the advantages of LDH, including size-adjustable nanochannels, excellent stability, etc., still give great possibilities to achieve higher lithium-magnesium separation effect. In particular, this simple and green method for preparing LDH nanosheets in large quantities provides the possibility for large-scale preparation of 2D layered membranes.

Theoretical calculations

The selective transport of ions across the membrane was investigated through theoretical calculations, focusing on the impact of channel size and charged properties on ion permeability. In particular, the interlayer channels of the LDH membrane have a diameter of about 0.3 nm, which introduces a degree of ion selectivity based on the different ability of each ion to penetrate these channels. In solution, ions are typically hydrated by six water molecules (Figure 9a, b), with Li^+ and Mg^{2+} having respective hydration diameters of 0.65 nm and 0.86 nm. To cross the channel, ions must be dehydrated. Easily dehydrated ions are more likely to pass through the sub-nanochannels of the membrane. The binding energy between Mg^{2+} and H_2O was found to be more significant (Figure 9c), suggesting that Mg^{2+} is less likely to dehydrate. Therefore, it is inferred that Mg^{2+} has lower permeability across the sub-nanochannels of the membrane compared to Li^+.

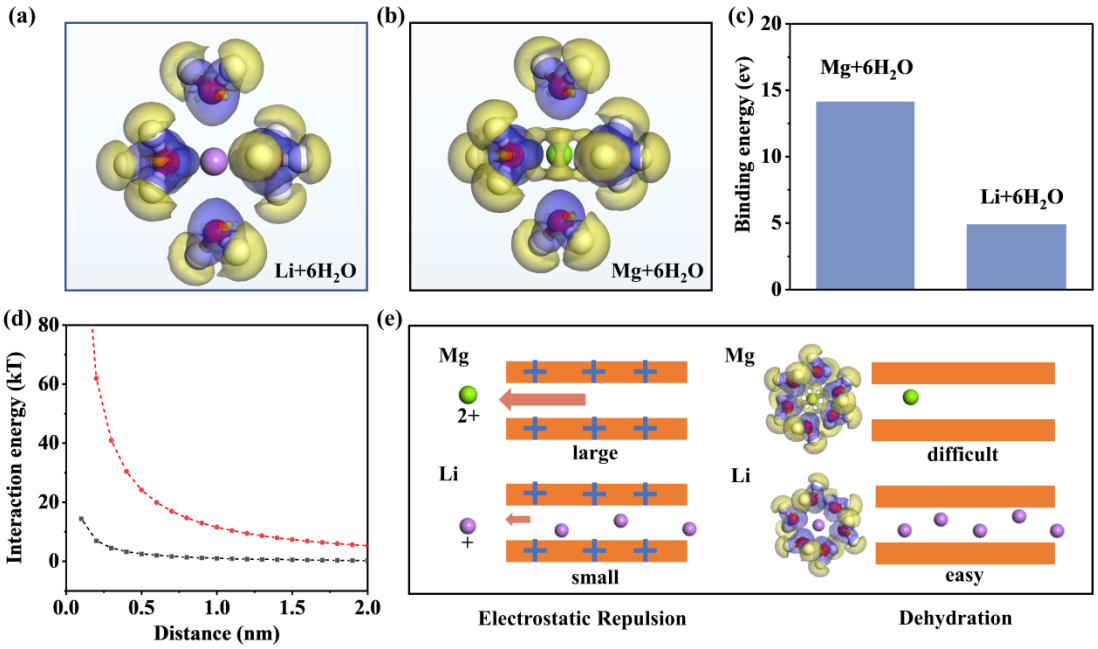

Figure 9. Electron density difference about (a) hydrated lithium ions and (b) hydrated magnesium ions; (c) the binding energy of lithium ions and magnesium ions with six H_2O; (d) Surface element integration model predictions of electrostatic repulsive force of the charged membrane surface against Mg^{2+} and Li^{+}; (e) Schematic of ion selective transport in the membrane caused by the difference of electrostatic repulsion and dehydration energy.

The separation of lithium and magnesium can be attributed to the positively charged characteristics of the membrane surface. The electrostatic double-layer interaction reflects the electrostatic repulsive force of the charged membrane surface against co-ions. To calculate the interaction energy between ions and the membrane surface, the interaction energy per unit area was integrated. Comparing the interaction energies of Mg^{2+} and Li^{+} with the LDH membrane surface, as depicted in Figure 9d, the membrane surface repels Mg^{2+} more strongly than Li^{+}. This finding is further supported by the observation of the higher rejection to Fe^{3+} in the experiment. Therefore, the charge effect and size sieving contribute to the lithium-magnesium separation effect of the membrane, as shown in Figure 9e.

Conclusion

In conclusion, a simple one-step method was used to synthesize micron-sized nitrate LDHs with only ~25 nanometers thickness. The study reveals a close relationship between the metal elements in LDHs laminates and the purity and size of synthesized nitrate LDHs. Zn and Al lamellar elements favored the synthesis of nitrate LDHs, resulting in larger particle sizes. The synthesized ZnAl-LDH can be directly exfoliated into nanosheets in formamide. This strategy offers advantages such as quick, low cost, and large size production of nanosheets, thereby providing the possibility for the large-scale preparation of 2D layered membranes. The LDH nanosheets were used to construct LDH layered membranes for lithium-magnesium separation, which exhibit stable lithium-magnesium separation ability with a separation ratio of Li/Mg of up to 6. The stability of LDH membrane in water and its positively charged characteristics contributed to the excellent stability of the separation ratio. This environmentally friendly method offers a simple strategy for large-scale preparation of LDH nanosheets and verifies the great potential of LDH lamellar membranes in lithium-magnesium separation. Compared with other methods of producing membranes from other 2D materials, which require complex processing to meet certain lithium-magnesium separation requirements, this strategy produces stable LDH membranes with minimum processing, making it a highly practical approach for industrial-scale applications.

Acknowledgements. This work was supported by the National Key Research and Development Program of China (2019YFC1806203) and the Fundamental Research Funds for the Central Universities (XK1802-6, BHYC1702B, and XK1803-05).

Data Availability and Reproducibility Statement: The data that support the findings of this study are available from the corresponding author upon reasonable request. The numerical data from Figures 1, 2, 5c, 6a, 7a, 7b, 9d and Figures S1, S14b are available as a .zip file in the Supplementary Material.

References

1. Li Z, Li C, Liu X, et al. Continuous electrical pumping membrane process for seawater lithium mining. *Energy Environ. Sci.* 2021;14:3152-3159.
2. Warnock SJ, Sujanani R, Zofchak ES, et al. Engineering Li/Na selectivity in 12-Crown-4–functionalized polymer membranes. *Proc. Natl. Acad. Sci.* 2021;118(37):e2022197118.
3. Bing S, Xian W, Chen S, et al. Bio-inspired construction of ion conductive pathway in covalent organic framework membranes for efficient lithium extraction. *Matter.* 2021;4(6):2027-2038.
4. Razmjou A, Asadnia M, Hosseini E, Habibnejad Korayem A, Chen V. Design principles of ion selective nanostructured membranes for the extraction of lithium ions. *Nat. Commun.* 2019;10(1):5793.
5. Li Z, Binnemans K. Opposite selectivities of tri-n-butyl phosphate and Cyanex 923 in solvent extraction of lithium and magnesium. *AICHE J.* 2021;67(7):e17219.
6. Swain B. Recovery and recycling of lithium: A review. *Sep. Purif. Technol.* 2017;172:388-403.
7. Li Z, Binnemans K. Selective removal of magnesium from lithium-rich brine for lithium purification by synergic solvent extraction using β-diketones and Cyanex 923. *AIChE J.* 2020;66(7):e16246.
8. Xin W, Lin C, Fu L, et al. Nacre-like Mechanically Robust Heterojunction for Lithium-Ion Extraction. *Matter.* 2021;4(2):737-754.
9. Wang K, Wang X, Januszewski B, et al. Tailored design of nanofiltration membranes for

water treatment based on synthesis-property-performance relationships. *Chem. Soc. Rev.* 2022;51(2):672-719.

10. Zhang Y, Wang L, Sun W, Hu Y, Tang H. Membrane technologies for Li^+/Mg^{2+} separation from salt-lake brines and seawater: A comprehensive review. *J. Ind. Eng. Chem.* 2020;81:7-23.

11. Ahmadi H, Zakertabrizi M, Hosseini E, et al. Heterogeneous asymmetric passable cavities within graphene oxide nanochannels for highly efficient lithium sieving. *Desalination.* 2022;538:115888.

12. Wang S, Yang L, He G, et al. Two-dimensional nanochannel membranes for molecular and ionic separations. *Chem. Soc. Rev.* 2020;49(4):1071-1089.

13. Wang J, Zhang Z, Zhu J, et al. Ion sieving by a two-dimensional $Ti_3C_2T_x$ alginate lamellar membrane with stable interlayer spacing. *Nat. Commun.* 2020;11(1):3540.

14. Zhang WH, Yin MJ, Zhao Q, et al. Graphene oxide membranes with stable porous structure for ultrafast water transport. *Nat. Nanotechnol.* 2021;16:337–343.

15. Li ZK, Wei Y, Gao X, et al. Antibiotics Separation with MXene Membranes Based on Regularly Stacked High-Aspect-Ratio Nanosheets. *Angew. Chem. Int. Ed. Engl.* 2020;59(24):9751-9756.

16. Zhu J, Wang L, Wang J, et al. Precisely Tunable Ion Sieving with an Al_{13}-$Ti_3C_2T_x$ Lamellar Membrane by Controlling Interlayer Spacing. *ACS Nano.* 2020;14(11):15306-15316.

17. Ren CE, Hatzell KB, Alhabeb M, Ling Z, Mahmoud KA, Gogotsi Y. Charge-and Size-Selective Ion Sieving Through $Ti_3C_2T_x$ MXene Membranes. *J. Phys. Chem. Lett.* 2015;6(20):4026-4031.

18. Zhang M, Guan K, Ji Y, Liu G, Jin W, Xu N. Controllable ion transport by surface-charged graphene oxide membrane. *Nat. Commun.* 2019;10(1):1253.

19. Sun Y, Yi F, Li RH, et al. Inorganic–Organic Hybrid Membrane Based on Pillararene‐Intercalated MXene Nanosheets for Efficient Water Purification. *Angew. Chem. Int. Ed.* 2022;134:e202200482.

20. Lu Z, Wu Y, Ding L, Wei Y, Wang H. A Lamellar MXene ($Ti_3C_2T_x$)/PSS Composite

Membrane for Fast and Selective Lithium-Ion Separation. *Angew. Chem. Int. Ed.* 2021;60(41):22265-22269.

21. Razmjou A, Eshaghi G, Orooji Y, et al. Lithium ion-selective membrane with 2D subnanometer channels. *Water Res.* 2019;159:313-323.

22. Lu D, Ma T, Lin S, et al. Constructing a selective blocked-nanolayer on nanofiltration membrane via surface-charge inversion for promoting Li^+ permselectivity over Mg^{2+}. *J. Membr. Sci.* 2021;635:119504,.

23. Li X, Zhang C, Zhang S, Li J, He B, Cui Z. Preparation and characterization of positively charged polyamide composite nanofiltration hollow fiber membrane for lithium and magnesium separation. *Desalination.* 2015;369:26-36.

24. Zhang H-Z, Xu Z-L, Ding H, Tang Y-J. Positively charged capillary nanofiltration membrane with high rejection for Mg^{2+} and Ca^{2+} and good separation for Mg^{2+} and Li^+. *Desalination.* 2017;420:158-166.

25. Xu P, Wang W, Qian X, et al. Positive charged PEI-TMC composite nanofiltration membrane for separation of Li^+ and Mg^{2+} from brine with high Mg^{2+}/Li^+ ratio. *Desalination.* 2019;449:57-68.

26. Gu T, Zhang R, Zhang S, et al. Quaternary ammonium engineered polyamide membrane with high positive charge density for efficient Li^+/Mg^{2+}separation. *J. Membr. Sci.* 2022;659:120802.

27. Lu Z, Wei Y, Deng J, Ding L, Li ZK, Wang H. Self-Crosslinked MXene ($Ti_3C_2T_x$) Membranes with Good Antiswelling Property for Monovalent Metal Ion Exclusion. *ACS Nano.* 2019;13(9):10535-10544.

28. Yeh CN, Raidongia K, Shao J, Yang QH, Huang J. On the origin of the stability of graphene oxide membranes in water. *Nat. Chem.* 2014;7(2):166-170.

29. Xu X, Wang J, Zhou A, et al. High-efficiency CO_2 separation using hybrid LDH-polymer membranes. *Nat. Commun.* 2021;12(1):3069.

30. Hu J, Tang X, Dai Q, et al. Layered double hydroxide membrane with high hydroxide conductivity and ion selectivity for energy storage device. *Nat. Commun.* 2021;12(1):3409.

31. Yu J, Wang Q, O'Hare D, Sun L. Preparation of two dimensional layered double

hydroxide nanosheets and their applications. *Chem. Soc. Rev.* 2017;46(19):5950-5974.

32. Wang Z, Yan X, Hou Q, et al. Scalable high yield exfoliation for monolayer nanosheets. *Nat. Commun.* 2023;14(1):236.

33. Shi K, Xu X, Dong S, Li B, Han J. Stretchable gas barrier films achieved by hydrogen‐bond self‐assembly of nano‐brick multilayers. *AIChE J.* 2021;67(10):e17373.

34. Yan Y, Liu Q, Wang J, et al. Single-step synthesis of layered double hydroxides ultrathin nanosheets. *J. Colloid Interface Sci.* 2012;371(1):15-19.

35. Chi H, Dong J, Li T, et al. Scaled-up synthesis of defect-rich layered double hydroxide monolayers without organic species for efficient oxygen evolution reaction. *Green Energy & Environment.* 2022;7(5):975-982.

36. Chen M, Zhu R, Lu X, Zhu J, He H. Influences of Cation Ratio, Anion Type, and Water Content on Polytypism of Layered Double Hydroxides. *Inogr. Chem.* 2018;57(12):7299-7313.

37. Tavares SR, Haddad JFS, Ivo R. Moraes P, Leitão AA. Computational exploration of the anion exchange on the basal surface of layered double hydroxides by molecular dynamics. *Appl. Surf. Sci.* 2020;513:145743.

38. Li K, Wang G, Duan X et al. Intercalation Assembly Method and Intercalation Process Control of Layered Intercalated Functional Materials. *Chin. J. Chem. Eng.* 2013;21(4):453-462.

39. Fu Y, Chen L, Ke J, et al. Simulate the diffusion of hydrated ions by nanofiltration membrane process with random walk. *Mol. Simulat.* 2012;38(6):491-497.

40. Dou Y, Pan T, Xu S, et al. Transparent, ultrahigh-gas-barrier films with a brick-mortar-sand structure. *Angew. Chem. Int. Ed. Engl.* 2015;54(33):9673-9678.

41. Chen H, Zhang F, Chen T, et al. Comparison of the evolution and growth processes of films of M/Al-layered double hydroxides with M=Ni or Zn. *Chem. Eng. Sci.* 2009;64(11):2617-2622.